Astroparticle Physics 168 (2025) 103089

Contents lists available at ScienceDirect

Astroparticle Physics

journal homepage: www.elsevier.com/locate/astropartphys

The time evolution of the low-energy deuteron fluxes measured in Cosmic Rays with the PAMELA experiment from the 23rd solar minimum to the 24th solar maximum

A. Lenni [1,2], M. Boezio [2,3], R. Munini [2,3],*, W. Menn [4], N. Marcelli [5], M.D. Ngobeni [6], D.C. Ndiitwani [6], I.I. Ramokgaba [6], M.S. Potgieter [7], O. Adriani [8,9], G.C. Barbarino [10,11], G.A. Bazilevskaya [12], R. Bellotti [13,14], E.A. Bogomolov [15], M. Bongi [8,9], V. Bonvicini [3], A. Bruno [16,17], F. Cafagna [14], D. Campana [11], P. Carlson [18], M. Casolino [19,20], G. Castellini [21], C. De Santis [19], A.M. Galper [22], S.V. Koldashov [22], S. Koldobskiy [23], A.N. Kvashnin [12], A.A. Leonov [22], V.V. Malakhov [22], L. Marcelli [19], M. Martucci [19], A.G. Mayorov [22], M. Mergè [24], E. Mocchiutti [3], A. Monaco [13,14], N. Mori [9], V.V. Mikhailov [25], G. Osteria [11], B. Panico [11], F. Palma [19], P. Papini [9], P. Picozza [19], M. Ricci [26], S.B. Ricciarini [9,21], M. Simon [4], A. Sotgiu [19], R. Sparvoli [19], P. Spillantini [27], Y.I. Stozhkov [12], A. Vacchi [3,28], E. Vannuccini [9], S.A. Voronov [22], Y.T. Yurkin [22], G. Zampa [3], N. Zampa [3]

[1] *University of Trieste, Department of Physics, I-34100 Trieste, Italy*
[2] *IFPU, I-34014 Trieste, Italy*
[3] *INFN, Sezione di Trieste, I-34149 Trieste, Italy*
[4] *Universitat Siegen, Department of Physics, D-57068 Siegen, Germany*
[5] *University of Roma Torvergata, Department of Physics, I-00133 Rome, Italy*
[6] *North-West University, Centre for Space Research, 2520 Potchefstroom, South Africa*
[7] *Institute for Experimental and Applied Physics, Christian-Albrechts University in Kiel, 24118 Kiel, Germany*
[8] *University of Florence, Department of Physics, I-50019 Sesto Fiorentino, Florence, Italy*
[9] *INFN, Sezione di Florence, I-50019 Sesto Fiorentino, Florence, Italy*
[10] *University of Naples "Federico II", Department of Physics, I-80126 Naples, Italy*
[11] *INFN, Sezione di Naples, I-80126 Naples, Italy*
[12] *Lebedev Physical Institute, RU 119991, Moscow, Russia*
[13] *University of Bari, Department of Physics, I-70126 Bari, Italy*
[14] *INFN, Sezione di Bari, I-70126 Bari, Italy*
[15] *Ioffe Physical Technical Institute, RU 194021, St. Petersburg, Russia*
[16] *Heliophysics Division, NASA Goddard Space Flight Center, Greenbelt, MD, USA*
[17] *Department of Physics, Catholic University of America, Washington DC, USA*
[18] *KTH, Department of Physics, and the Oskar Klein Centre for Cosmoparticle Physics, AlbaNova University Centre, SE 10691, Stockholm, Sweden*
[19] *INFN, Sezione di Rome "Tor Vergata", I-00133 Rome, Italy*
[20] *RIKEN, EUSO team Global Research Cluster, Wako-shi, Saitama, Japan*
[21] *IFAC, I-50019 Sesto Fiorentino, Florence, Italy*
[22] *MEPhI: National Research Nuclear University MEPhI, RU 115409, Moscow, Russia*
[23] *University of Oulu, 90570 Oulu, Finland*
[24] *Agenzia Spaziale Italiana (ASI), IT 00133, Roma, Italy*
[25] *Shandong Institute of advanced technology, China*
[26] *INFN, Laboratori Nazionali di Frascati, Via Enrico Fermi 40, I-00044 Frascati, Italy*
[27] *Istituto Nazionale di Astrofisica, Fosso del cavaliere 100, 00133 Roma, Italy*
[28] *University of Udine, Department of Mathematics, Computer Science and Physics Via delle Scienze, 206, Udine, Italy*

ARTICLE INFO

Keywords:
Cosmic rays
Deuterons

ABSTRACT

The space-borne PAMELA experiment was launched on the 15th of June 2006 on board the Russian satellite Resurs-DK1 from the Baikonur Cosmodrome. The PAMELA instrument performed high-precision measurements of cosmic rays over a wide energy range until January 2016.

---

* Corresponding author at: INFN, Sezione di Trieste, I-34149 Trieste, Italy.
E-mail address: riccardo.munini@ts.infn.it (R. Munini).

https://doi.org/10.1016/j.astropartphys.2025.103089
Received 11 September 2024; Received in revised form 28 January 2025; Accepted 29 January 2025

Heliosphere
Solar activity cycle
Solar modulation

We present the yearly average deuteron spectra for the 23rd solar minimum (July 2006 – January 2009) and the first part of the 24th solar maximum (until September 2014). The deuterons were selected with a rigidity between 0.75 and 2.6 GV by combining the Time of Flight (ToF) and the tracker systems. The measured spectra display a rising trend toward the solar minimum followed by a decreasing trend as the solar maximum approaches. The corresponding deuteron-to-proton flux ratios show time dependence at the lowest rigidities, as expected due to the different charge-to-mass ratios and the different shapes of the respective local interstellar spectra. These results are significant for the fine-tuning of propagation and modulation models of cosmic rays through the heliosphere.

1. Introduction

Deuterium nuclei, also called deuterons, are rare isotopes in cosmic rays (CRs); they account only for about 3% of the hydrogen abundance in the cosmic radiation. Unlike protons, deuterons are generally believed to be of secondary origin; they are destroyed rather than created during stellar nucleosynthesis and generated from nuclear interactions of primary CRs with the galactic interstellar medium. In detail, deuterons are created mainly from the spallation of primary ^{4}He nuclei on protons ($^4\mathrm{He} + \mathrm{p} \rightarrow D + {}^3\mathrm{He}$) and from proton fusion processes ($\mathrm{p} + \mathrm{p} \rightarrow D + \pi^+$). Their spectral shape and fluxes are ultimately determined by the injection spectra of the primary parent elements, by the propagation mechanisms in the space environment, and by the cross-sections of their production processes. Therefore, the measurements of the galactic D spectrum are a powerful tool to constrain the parameters of theoretical models developed to describe CR propagation (e.g., Webber [1], Coste et al. [2], Tomassetti [3], Wu and Chen [4], Gomez-Coral et al. [5]).

Until the late 1990s, most galactic D fluxes (e.g., Webber et al. [6], de Nolfo et al. [7], Bogomolov et al. [8], Wang et al. [9],Papini et al. [10]) were obtained with instruments detecting CRs onboard stratospheric balloons. Most of these experiments were equipped with spectrometers with the mass resolution needed to reject the dominating primary background. However, their measurements were affected by a non-negligible background of secondary particles produced in the interactions of CRs with the residual layer of the atmosphere above the apparatus. The calculation of this background was challenging due to limited knowledge of the cross sections for the isotope production processes, resulting in substantial systematic errors affecting the measured deuteron fluxes. Measurements performed in space are free of these uncertainties (e.g., Aguilar et al. [11], Adriani et al. [12], Aguilar et al. [13]).

Because of the finite instrumental resolution of the detectors, the isotopic separation between protons and deuterons is usually performed on a limited energy range, typically from a few tens of MeV/nucleon up to a few GeV/nucleon. At these low energies, the CR propagation is strongly affected by the interaction with the turbulent solar wind and the embedded heliospheric magnetic field. The propagation through the heliosphere reduces the CR intensity and produces a time-dependent flux that is anti-correlated with the solar activity, which follows an 11-year cycle. This effect is called solar modulation (e.g., Potgieter [14], Bazilevskaya et al. [15]).

The satellite-borne experiment PAMELA (Payload for Antimatter Matter Exploration and Light-nuclei Astrophysics, Picozza et al. [16]) has been an ideal experiment for solar modulation studies; it operated for about ten years, comprising almost a whole solar cycle, and its semipolar orbit allowed it to measure low-energy particles, which are more affected by solar modulation. The PAMELA collaboration has already published several papers on solar modulation of CRs: protons [17,18], electrons [19], positron-to-electron flux ratio [20], and helium nuclei [21,22]. The PAMELA collaboration has also published data on the deuteron component [12,23], but these results were limited to the first two years (2006 and 2007) of data taking. Here, a new measurement of the time-dependent galactic CR deuteron fluxes measured by PAMELA between July 2006 and September 2014 is presented between 50 and 800 MeV/nucleon. This period is relevant for solar-modulation studies because it covers almost a whole solar cycle and includes a change in solar magnetic polarity in 2013. Precise time-dependent proton and deuteron flux measurements provide valuable information about possible diverse modulation effects due to different mass-to-charge ratios and different shapes of their local interstellar spectra (LIS).[1]

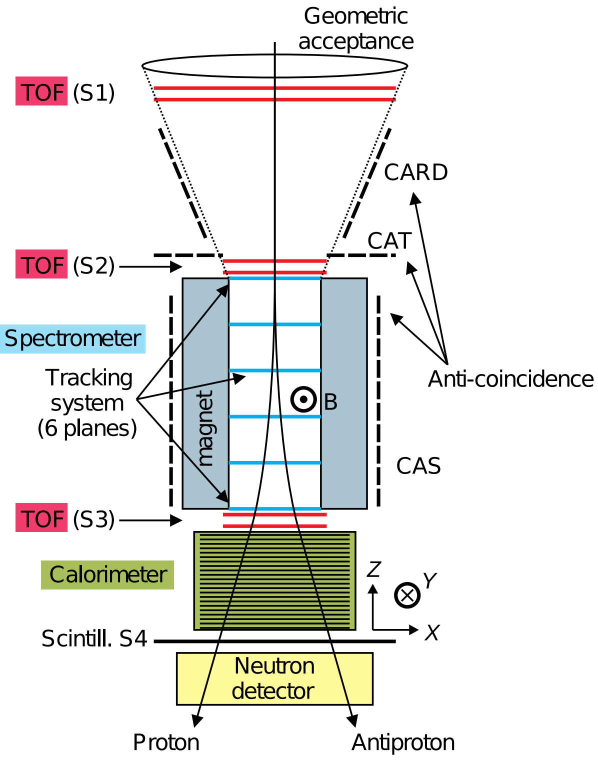

Fig. 1. A schematic overview of the PAMELA instrument and its detectors. The magnetic field lines in the spectrometer cavity are oriented along the y-direction.

2. The PAMELA experiment

The PAMELA instrument was an earth-orbiting detector designed to measure CRs in space. The PAMELA instrument was launched on the 15th of June 2006 from the Baikonur cosmodrome in Kazakhstan on board the Russian satellite Resurs DK1 and followed an elliptical and semipolar low-earth orbit with an inclination of 70° until 2010 at a height varying between 350 km and 610 km. Then, the orbit was modified to a circular one at an altitude of about 600 km, maintaining the same inclination.

A schematic view of the PAMELA experiment is shown in Fig. 1. The core of the apparatus was the magnetic spectrometer equipped with a tracker composed of six planes of double-face silicon microstrip detectors placed in a magnetic cavity to measure the trajectory of incoming particles. The spatial resolution is ~ 3 μm in the bending

---

[1] The energy spectrum of CRs as outside the Heliosphere.

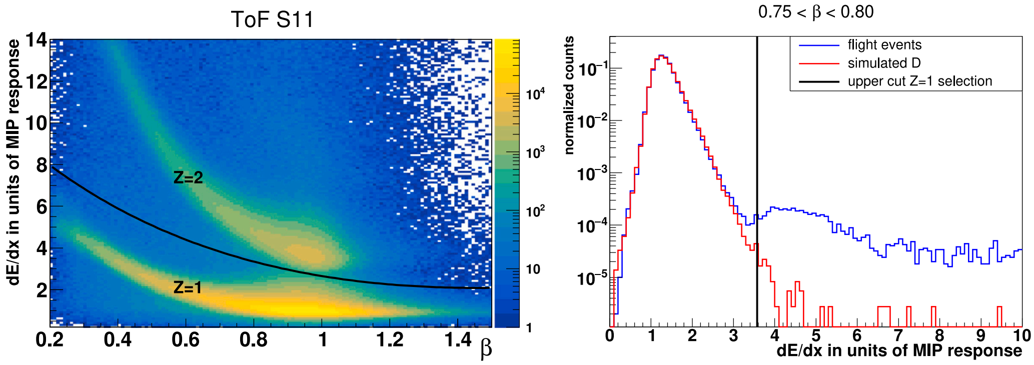

Fig. 2. Left panel: the $\mathrm{d}E/\mathrm{d}x$ distributions measured in the S11 TOF layer for events surviving criteria 1–6. The black curve indicate the upper limits of the $Z = 1$ selection. Right panel: the $\mathrm{d}E/\mathrm{d}x$ measured in the S11 TOF layer for events with $0.75 < \beta < 0.8$. The red histogram represents simulated deuterons while the blue represents flight events surviving criteria 1–6.

view (x-view) and ∼ 11 μm in the non-bending view (y-view). The spectrometer measured the magnetic rigidity ρ of the crossing particles, defined as $\rho = pc/Ze$, where p is the particle momentum, c the speed of light in vacuum and Ze the particle electric charge. The tracker also provided twelve $\mathrm{d}E/\mathrm{d}x$ measurements obtained by the six double-sided silicon planes. A Time-of-Flight (TOF) system was composed of six layers of fast plastic scintillators arranged in two planes above (named S1 and S2) and one plane below (named S3) the magnetic spectrometer as in Fig. 1. The TOF system triggered the data acquisition, measured the velocity of the crossing particle, and provided six independent $\mathrm{d}E/\mathrm{d}x$ measurements. A primary anti-coincidence (AC) system consisted of four plastic scintillators (CAS) surrounding the sides and one covering the top (CAT) of the magnetic spectrometer. A secondary AC system consisted of four plastic scintillators (CARD) surrounding the volume between the first two TOF planes. An electromagnetic calorimeter composed of 44 single-sided silicon sensor planes interleaved with 22 planes of tungsten was placed below the S3 plane. It provided discrimination between hadronic and electromagnetic showers and non-interacting particles, as well as multiple energy loss measurements. At the bottom of the apparatus, there were a shower tail catcher scintillator used to measure the shower leakage from the calorimeter and a neutron detector to improve the discrimination between hadronic and electromagnetic showers based on the measured number of neutrons generated in the calorimeter. The apparatus was enclosed in a pressurized container attached to the side of the Resurs-DK1 satellite. The total weight of PAMELA was 470 kg while the power consumption was 355 W. More detailed descriptions of the instruments and data handling can be found in Picozza et al. [16], Adriani et al. [24] and Adriani et al. [25].

The PAMELA experiment took data practically continuously until January 2016, covering almost an entire solar cycle, from the middle of the 23rd solar minimum to the middle of the 24th solar maximum. The data collected during this broad period represents an excellent opportunity to study the time evolution of the low-energy CR fluxes caused by solar modulation.

3. Data selection

The main focus of the deuteron selection was the rejection of the vast background represented mainly by protons, which are almost 30 times more abundant than deuterons. In the following, the deuteron selection is presented.

3.1. Event preselection

The following criteria were used to select a sample of positively and unitary charged particles with a single downward-going track well reconstructed inside the spectrometer:

Table 1
The parameters for the χ^2 cut described in the text.

χ^2 cut parameters				
p_0	p_1 (GV)	p_2 (GV^2)	p_3 (GV^3)	p_4 (GV^4)
1.8	0.95	2.49	−1.21	0.22

1. Only events outside the South Atlantic Anomaly were used, thus reducing multi-particle events due to the increased density of the trapped particles. The selection required the events were recorded where the Earth's magnetic field strength, evaluated with the 12th-generation International Geomagnetic Reference Field (IGRF-12) model [26], was not less than 0.26 G.
2. Reconstructed tracks had to be fully contained in the magnet cavity, i.e., 1.5 mm away from the walls of the magnetic spectrometer. This requirement rejected particles that interacted with the magnetic walls.
3. Reconstructed tracks were required to have a minimum of three hits in the tracker both on the x-view and y-view and a lever arm, defined as the minimum number of tracker layers between the first and the last hit, of at least four.
4. Tracks with a significant scattering in the tracker were rejected using the χ^2 value provided by the fit of the track. The cut was defined as:
$$\chi^2 < p_0 + p_1\eta + p_2\eta^2 + p_3\eta^3 + p_4\eta^4 \quad (1)$$
where η is the particle deflection defined as $\eta = 1/\rho$. The values of the 5 parameters in the equation were calibrated in order to have an almost constant efficiency at 95% over the entire energy range and are provided in Table 1.
5. Particles crossing the PAMELA apparatus from the top down and with a positive electric charge were selected requiring velocity $\beta > 0$ ($\beta = v/c$, v the measured velocity of the particle, c speed of light in vacuum) and $\rho > 0$.
6. Events were selected with no associated signal on the CARD and CAT detectors to reject multi-particle events, which typically activate these AC detectors.
7. The $\mathrm{d}E/\mathrm{d}x$ in MIP (Minimum Ionizing Particle) units measured in the first layer of the TOF system (top plane of S1 in Fig. 1) was used to select particles with electric charge $Z = 1$. As an example, Fig. 2 left panel shows the distribution of the $\mathrm{d}E/\mathrm{d}x$ values for S11 as a function of β as reconstructed by the TOF (values of β greater than 1 are due to the TOF resolution, e.g. see Adriani et al. [12]) for events selected with criteria 1–6. The black curve represents the selection upper limit for $Z = 1$ particles. Similar selections were performed on the $\mathrm{d}E/\mathrm{d}x$ distribution of the ToF plane S12, S21 and S22. This selection is also relevant to reject particles with $Z > 1$ that, fragmenting

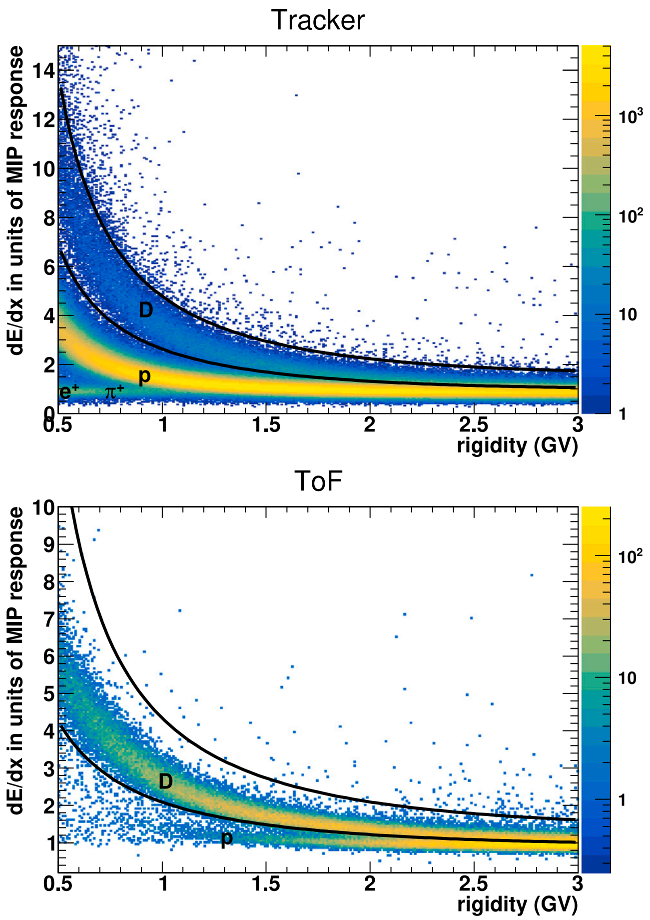

Fig. 3. Top panel: the distribution of the second lowest dE/dx measurement in the tracker as a function of rigidity for events surviving criteria 1–8. The black lines represent the cuts defined to select deuteron. Bottom panel: the distribution of the second lowest dE/dx measurement in the TOF system as a function of rigidity for the events surviving criteria 1–9. The black lines represent the deuteron selection cuts.

in the top TOF layers, may mimic unitary charged particles in the tracker. The right panel of Fig. 2 shows the S11 dE/dx for event with $0.75 < \beta < 0.8$. The red line represents simulated deuteron while the blue line represents the flight event surviving criteria 1–6. The Z=1 simulated and flight distributions are in good agreement.

8. Spatial consistency between the hits in the TOF paddles and the reconstructed track was required, further rejecting multi-particle events.

3.2. Isotopic separation

A sample of unitary charged particles (mostly protons, deuterons, and positrons) was selected after these criteria. Additional conditions, based on the dE/dx measurements in the TOF and the tracker layers, were employed to separate deuterons from protons.

For each event, several dE/dx measurements are available, up to 12 provided by the tracker and up to 6 by the TOF system. It was found that the second lowest dE/dx measurement provided the best information, significantly reducing the ionization-loss fluctuations and effects of noise.

Fig. 3 (top panel) shows the distribution of the second lowest dE/dx measurement in the tracker for the $Z = 1$ events selected with criteria 1–8 and collected in 2006. Protons and deuterons are distinguishable up to a value of about 1.5 GV. Above this rigidity, deuterons become progressively relativistic, and the two distributions start to overlap. A few triton events can be seen above the deuteron distribution; these events were not of galactic origin but were generated from the fragmentation of heavier nuclei interacting with the PAMELA apparatus. Moreover, a small component of positrons and positively charged pions (the latter produced locally) is present at the lower rigidities with low dE/dx values. Consequently, deuterons were selected as follows.

9. Events were selected if the tracker's second lowest dE/dx measurement was included in the band defined by the solid lines in Fig. 3 (top panel).

This selection removed the bulk of the proton contamination up to a rigidity of about 1.5 GV. Above 1.5 GV, a selection based on the TOF second lowest dE/dx measurement was used. Fig. 3 (bottom panel) shows this quantity for events surviving criteria 1–9. Hence,

10. Events were selected if the TOF second lowest dE/dx measurement was included in the band defined by the solid lines in Fig. 3 (bottom panel).

The combined use of criteria 9 and 10 extended the rigidity range up to around 2 GV with a negligible proton background. The energy range was further extended using the β information. Fig. 4 shows the $1/\beta$ distribution obtained with event collected in 2006 and selected with criteria 1–8 (left) and with criteria 1–10 (right). Above 2 GV, the deuteron component was estimated with a double Gaussian fit of this quantity in each rigidity bin. Since the velocity is inversely proportional to the time measured by the TOF system, the resolution of $1/\beta$ can be approximated with a Gaussian. Fig. 5 shows the $1/\beta$ values of the events selected with criteria 1 to 10 for three different rigidity bins between 2.1 and 2.6 GV. The total number of events selected in the rigidity bin is N_{tot}. The double Gaussian fit (orange line in the figure) to the data provided an estimation of the number of protons N_p and deuterons N_D. The only free parameters of the fit procedure were the normalization factors. The mean and sigma values of the two Gaussians were obtained for each rigidity interval by fitting the corresponding $1/\beta$ distributions for samples of protons and deuterons selected using the dE/dx measured in the calorimeter for non-interacting particles, as described in Adriani et al. [12]. The integral of the double-Gaussian distribution systematically underestimated the total number of events. This discrepancy was constant, at about 2%, and the estimated number of deuterons was increased by this value. The discrepancy was also used for the calculation of the systematic uncertainty.

Deuterons were selected up to 2.6 GV. Above this rigidity, the proton and deuteron Gaussian means differed less than their FWHM, and the uncertainties on the estimated number of events became greater than 10%.

4. Flux determination

Deuterons were selected with the described criteria for each calendar year from June 2006 until September 2014. Because of the broad geomagnetic region spanned by the PAMELA experiment during its orbit, deuterons were selected over seven vertical geomagnetic cut-off intervals estimated using the Resurs-DK1 satellite position and the Störmer approximation. The cut-off rigidity intervals of the geomagnetic cut-off slices adopted in the analysis are listed in Table 2.

The counts of the selected events in each geomagnetic cut-off interval were corrected for the selection efficiencies, the particle losses, the contamination from production of secondary deuteron inside the apparatus, and the energy losses. These corrections were evaluated using a Monte Carlo simulation of the PAMELA instrument based on the GEANT4 code [27] and using the flight data as described in the following. The simulation accurately reproduced the geometry and performance of the PAMELA detectors. The simulation code was validated by comparing the distributions of several significant variables with those obtained from flight data. Hadronic interactions were handled via the QGSP_BIC_HP physics list for all the isotopes under study.

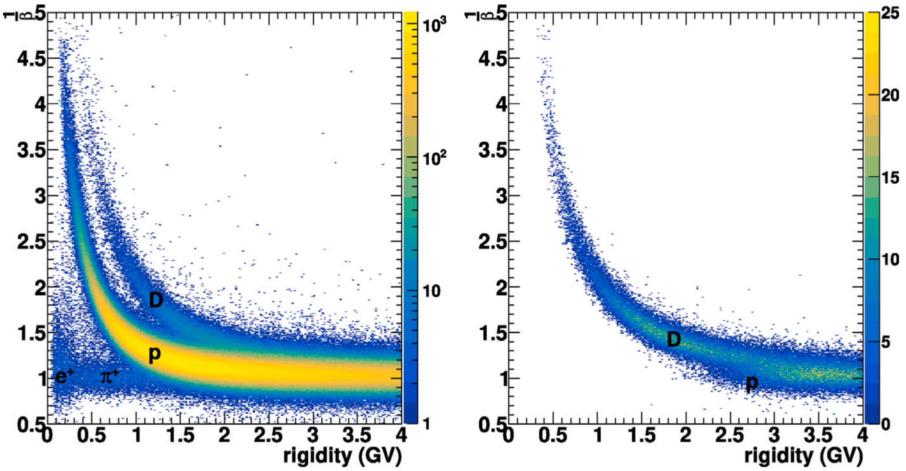

Fig. 4. The $1/\beta$ distribution for events collected in 2006 and selected, left: with criteria 1–8; right: with criteria 1–10.

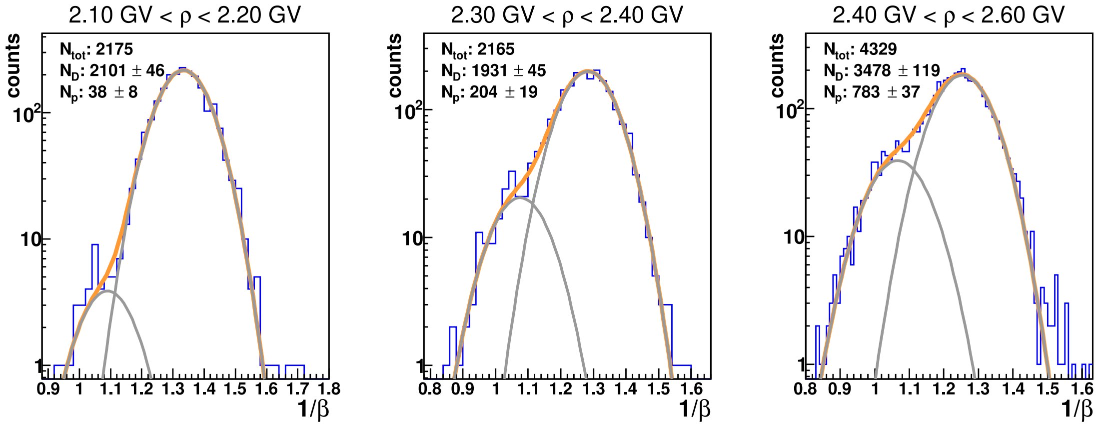

Fig. 5. The $1/\beta$ distribution for events selected in three rigidity bins after selection criteria 1–10 for 2006 chosen as an example. The double Gaussian fit is shown with the estimated number of protons and deuterons.

Table 2
Division in geomagnetic cut-off slices.

Geomagnetic cut-off rigidity intervals	
1st slice	0.00–0.38 GV
2nd slice	0.38–0.535 GV
3rd slice	0.535–0.69 GV
4th slice	0.69–1.153 GV
5th slice	1.153–1.46 GV
6th slice	1.46–1.84 GV
7th slice	1.84–2.3 GV

4.1. Selection efficiencies

The selection (from criterion 3 on) efficiencies were estimated following the order shown in Sections 3.1 and 3.2. E.g., criterion 9 was evaluated using a sample selected with criteria 1 to 8. If additional conditions were required to select a clean sample of particles, simulation was used to study the presence of possible biases. Simulated deuteron samples were also used to obtain the efficiencies related to the track reconstruction (criteria 3–5) and their rigidity dependence since only the magnetic spectrometer provided rigidity measurements. Considering the simulation provides the rigidity at the top of the instrument ρ_0, before any energy loss, these simulated efficiencies were evaluated as a function of ρ_0 and applied after unfolding the spectrum to the top of the instrument (procedure described in Section 4.4).

A notable change is observed over time in the tracking efficiency, decreasing from around 90% in 2006 down to 20% in 2014 as an effect of a decline in the tracker performance. This degradation, included in the simulation, was due to progressively random failure of some readout electronic chips connected to the microstrip detectors in flight, which created dead areas over the silicon planes.

As initially described, the efficiencies of the other criteria (6–10) were studied individually and in sequence with simulated and flight data, exploiting the redundant information provided by the PAMELA detectors. First, the efficiencies of these criteria were obtained using simulated data. Then, efficiency samples were extracted from flight and simulated data using additional selection criteria optimized to minimize the proton contamination in the flight samples over a wide rigidity range. These additional selections were based on the measured TOF β (called criterion 11) and the detected $\mathrm{d}E/\mathrm{d}x$ deposits in the calorimeter (called criterion 12) for non-interacting events. The resulting experimental and simulated efficiencies were compared, where different, correction factors were estimated Finally, these correction factors were applied to the original simulated efficiencies, thus accounting for possible biases in the experimental efficiency samples. Fig. 6 shows this procedure applied to the efficiencies for criterion 9.

For each criterion, the yearly averaged efficiency was evaluated for each year of the analysis to account for possible time variation of the detector responses.

4.2. Residual background

The residual proton contamination was estimated by selecting protons using the β and calorimeter $\mathrm{d}E/\mathrm{d}x$ information for non-interacting

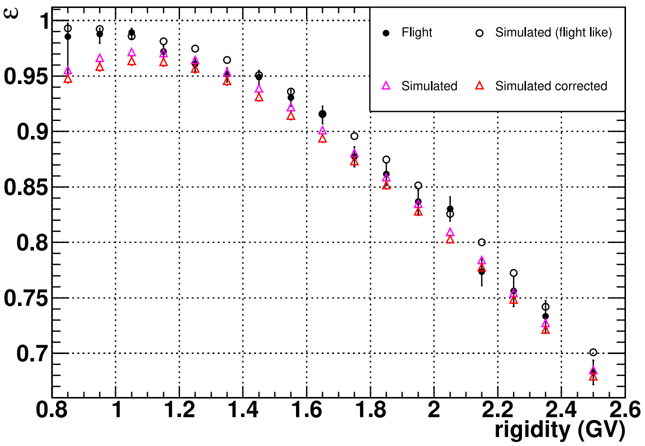

Fig. 6. Efficiencies calculated for criterion 9 using a flight sample selected with criteria 1–8 plus 11–12 (black dots), using a simulated efficiency sample selected with criteria 1–8 plus 11–12 (black circles), simulated efficiencies using a sample selected with criteria 1–8 (magenta triangles) and corrected for the discrepancy between flight and simulated efficiencies (red triangles).

events. The fraction of these events passing criteria 9 and 10 provided the proton residual contamination for these criteria. Up to 1.7 GV, the surviving proton fraction was lower than 2×10^{-5}; at higher rigidities, the surviving fraction gradually rose to 9×10^{-4} at 2.5 GV. Since the galactic proton flux is about two orders of magnitude greater than the deuteron flux, the residual proton contamination was lower than 10^{-3} up to 2 GV. At higher rigidities, the double-gaussian fit of the $1/\beta$ distributions provided the deuterons and protons counts, with fit errors providing the related uncertainties.

The rejection of $Z > 1$ events was given mostly by criterion 7, based on the ionization losses by particles traversing the TOF S1 and S2 scintillators. The residual background of heavier nuclei in the deuteron sample was estimated by calculating the rejection capability of each of the two sets of TOF scintillators. First, using $Z > 1$ particles selected with the ionization losses in S21 and S22 scintillators, the fraction of the heavier nuclei surviving the $Z = 1$ selection based on the ionization losses in the S1 scintillators was derived. The resulting fraction decreased from around 10^{-2} below 1 GV down to 2×10^{-4} above 1.5 GV. Similarly, the fraction of heavier nuclei surviving the $Z = 1$ selection based on the ionization losses in the S2 scintillators was obtained using $Z > 1$ particles selected with the ionization losses in S11 and S12 scintillators. The resulting fraction of $Z > 1$ particles decreased from 10^{-2} at 1.1 GV down to 10^{-3} above 1.5 GV. The residual contamination of $Z > 1$ events in the final sample of deuterons was obtained by multiplying the two estimated contaminations. At low rigidities, it was estimated that out of 10^4 events selected as deuterons, fewer than one was a helium nucleus. Above 1.4 GV, this residual contamination decreased to one helium nuclei out of 10^6 selected events. This procedure was validated using the simulation; hence, the contamination was assumed to be negligible over the whole rigidity range under analysis.

4.3. Contamination from inelastic scattering of nuclei

Inelastic scattering of nuclei with the PAMELA apparatus could produce secondary D nuclei then passing the deuteron selection. This contamination was studied with the simulation, and it was found that the contribution to secondary deuterons produced by the fragmentation of ^{3}He and higher charge nuclei and by the spallation of atoms from the apparatus induced by the incoming cosmic protons was more than an order of magnitude lower than the contamination due to ^{4}He nuclei. Hence, it was neglected in favor of the contamination caused by ^{4}He nuclei, estimated as described in the following.

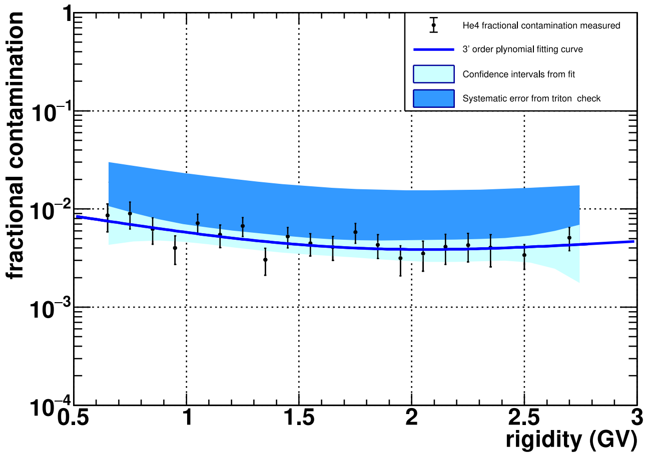

Fig. 7. Fractional contamination from ^{4}He fragmentation in the final D sample. See text for details.

A sample of ^{4}He nuclei was simulated entering isotropically the PAMELA apparatus. Since criterion 7 discarded events with $Z = 1$ produced by interactions of heavier nuclei with the TOF layers above the magnetic spectrometer, the residual contamination from ^{4}He nuclei came essentially from inelastic interactions with the 2 mm aluminum dome covering the PAMELA instrument. To properly account for the contamination of locally produced deuterons, the number of simulated ^{4}He events had to be equalized to the experimentally recorded data. This scaling was performed using the flight data collected in 2006 and selecting ^{4}He similarly in the flight and simulation data. The ^{4}He events were chosen with selections including criteria 1–6 plus a He-selecting condition on the tracker $\mathrm{d}E/\mathrm{d}x$ distribution as a function of the rigidity. Finally, the $1/\beta$ distribution of each rigidity interval was fit with a double Gaussian distribution to account for and reject the ^{3}He nuclei, abundantly present in the flight data [12]. Flight data events were also required to belong to the first geomagnetic cut-off slice to reject re-entrant albedo particles. The scaling factor was calculated as a function of the kinetic energy per nucleon. This dependence was chosen because the kinetic energy per nucleon is conserved during the fragmentation and spallation process, allowing the application of the same scaling factor to the counts of the fragmentation products, like deuterons, in simulation. Since no energy dependence was observed, a constant scaling factor was applied to the simulated secondary particles produced in ^{4}He nuclei fragmentation.

Finally, the number of deuterons in the flight data produced by the fragmentation of ^{4}He was estimated as follows. The $1/\beta$ distributions of the simulated events, selected with criteria 1–10 in each rigidity interval, were fitted with a double Gaussian, and the resulting numbers of deuterons were multiplied by the corresponding scaling factors. The estimated deuteron counts were compared with the deuteron counts obtained from flight data in the first geomagnetic cut-off slice. The resulting fractional contaminations, defined as F_c, due to fragmentation of ^{4}He are shown in Fig. 7. The pale blue shaded area depicts the confidence intervals from a third-order polynomial fit and shows less than 1% contamination in the whole rigidity range. The deuteron counts from flight data were multiplied by $1 - F_c$, providing the counts for the deuteron flux calculation.

The reliability of the modeling of the processes of ^{4}He fragmentation and secondary particle production in the simulation was validated by comparing the triton counts found in the ^{4}He simulations, corrected for the scaling factor, and in the flight data. Galactic tritons cannot survive the propagation in the Galaxy due to their short half-life time. Thus, all tritons detected in the flight data had to be generated from the local fragmentation of heavier nuclei, mainly ^{4}He. Tritons were selected in simulated and flight data with conditions including criteria

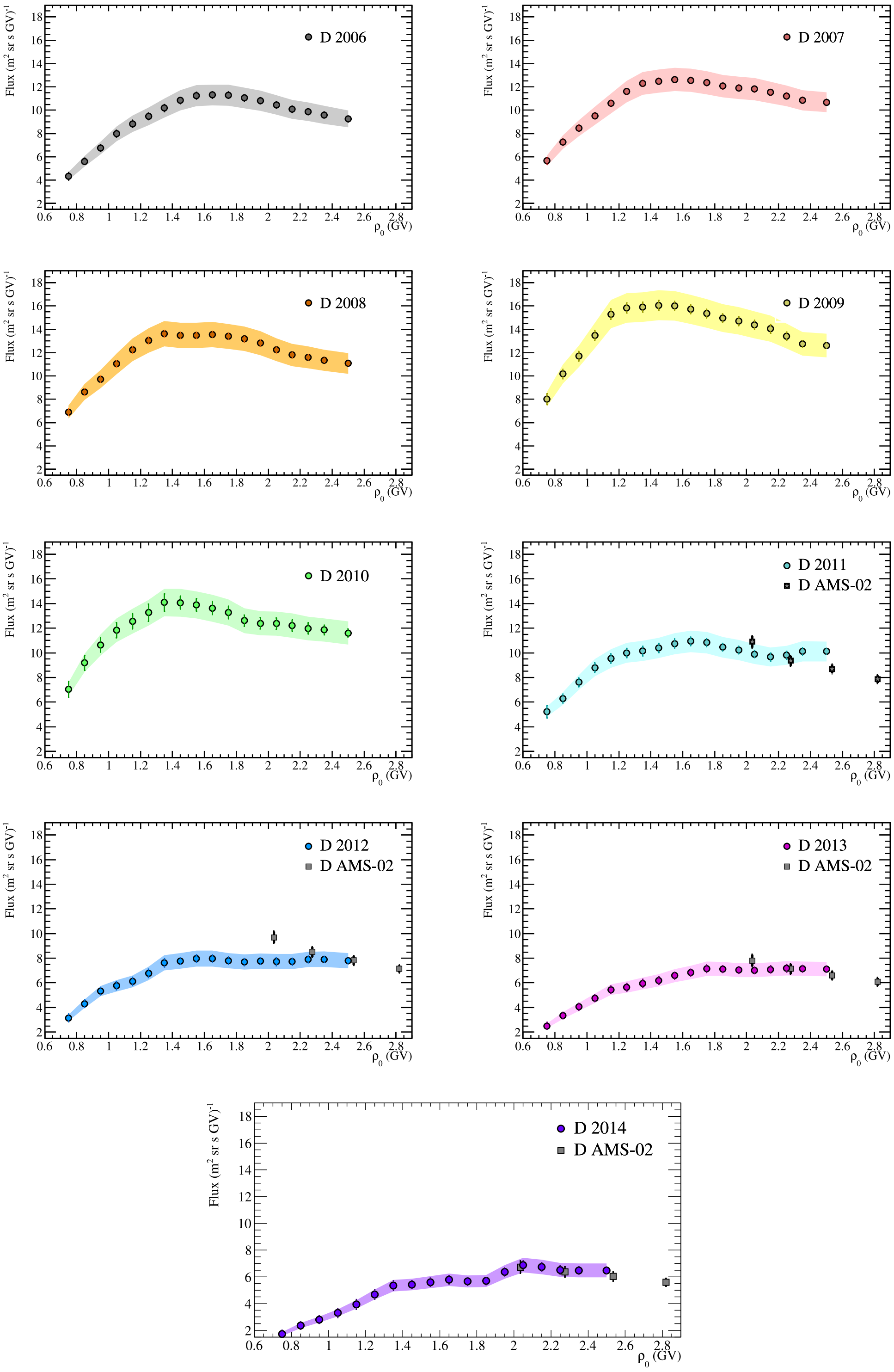

Fig. 8. Yearly average D spectra measured by PAMELA from 2006 to 2014 (colored points). Not visible statistical errors bars are smaller than the symbols. The shaded area represents the systematic uncertainties. The comparison with the AMS-02 (gray squares) data [13] is shown.

1–8, a cut on the tracker dE/dx distribution, and a triple Gaussian fit applied on the $1/\beta$ distributions of each rigidity bin. The ratios of the simulated to flight triton numbers were found to be constant, with an average value of 0.25. This value pointed to an underestimation of the triton production in the simulation, probably due to inaccurate modeling of the physical processes involved in the ^{4}He fragmentation and subsequent triton fusion process within the GEANT4 simulation. Different physics lists were used to reproduce the process, but all reported the same issue. Protons, ^{3}He nuclei, and heavier nuclei were also generated and analyzed, finding that they produced a negligible amount of tritons. The disagreement between flight and simulated triton counts was taken into account as a systematic uncertainty (see

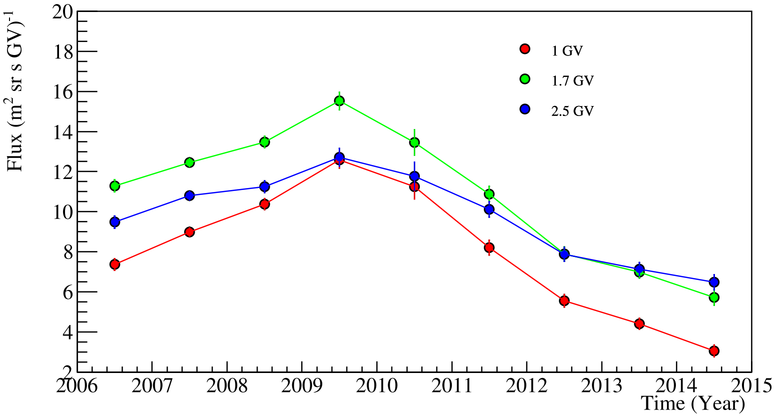

Fig. 9. The D flux as a function of time for three different rigidity values.

Section 5) affecting the secondary particle production from ^{4}He fragmentation in the simulation. This uncertainty is shown in Fig. 7 as a blue band in Fig. 7.

4.4. Unfolding procedure

The finite resolution of the magnetic spectrometer and the particle slowdown due to ionization energy losses make the measured rigidity ρ differ from the actual rigidity value at the top of the instrument ρ_0, with consequent distortion of the particle spectrum. An iterative Bayesian unfolding method proposed by D'Agostini [28] was used to correct this effect and reconstruct statistically the selected deuteron counts as a function of ρ_0 (see Supplementary Material of Adriani et al. [29]). A detector response matrix was calculated with Monte Carlo data, one for each year under analysis.

The unfolding procedure was applied to the count distributions of selected deuterons binned according to their measured rigidities and divided by all selection efficiencies except those of the tracking system. Subsequently, the track reconstruction efficiency was applied to the unfolded count.

4.5. Live time

The live time was provided by an onboard clock that measured the time during which the PAMELA apparatus was waiting for a trigger. The live time was determined for each of the seven geomagnetic cut-off slices (outside the South Atlantic Anomaly) and each rigidity bin. The accuracy of the live time, cross-checked by comparing different clocks available in flight, was observed to have a relative difference of less than 0.2% [17].

4.6. Geometrical factor and hadronic interactions

The PAMELA nominal geometrical factor G_F was determined in simulation with requirements of triggering and containment within the fiducial volume (criterion 2). G_F is almost constant above 1 GV with a value of 19.9 cm^2 sr and slowly decreases by $\sim$ 2% to lower energies, as an effect of the bending of the particle track within the magnetic spectrometer.

Deuterons may be lost because of hadronic interactions in the 2 mm thick aluminum pressurized container covering PAMELA. This effect was included in the PAMELA geometrical factor as follows:

$$G(\rho_0) = [1 - b(\rho_0)]G_F(\rho_0) \tag{2}$$

where $G(\rho_0)$ is the effective geometrical factor that was used for the flux calculation, and $b(\rho_0)$ is a correction factor that accounted for the effect of inelastic scatterings. This correction factor $b(\rho_0)$ was obtained from Monte Carlo simulation and makes $G(\rho_0)$ 10% lower than G_F.

4.7. Flux calculation

The particle flux $\phi(\rho_0)$ was calculated, as a function of the rigidity at the top of the instrument, for each geomagnetic cut-off interval as:

$$\phi(\rho_0) = \frac{N\left(\rho_0\right)}{G\left(\rho_0\right) \cdot T \cdot \epsilon\left(\rho_0\right) \cdot \Delta\rho_0} \tag{3}$$

where $N\left(\rho_0\right)$ is the sum of the unfolded number of deuteron events, $\Delta\rho_0$ is the width of the rigidity interval, $\epsilon\left(\rho_0\right)$ is the track reconstruction efficiency $G\left(\rho_0\right)$ is the geometrical factor, and T is the sum of the live times of the used geomagnetic cut-off intervals. The fluxes estimated in rigidity regions at least 1.3 times above the maximum vertical geomagnetic cut-off of each interval were assumed to be of galactic origin. Finally, the deuteron spectrum was determined by combining the resulting fluxes of each geomagnetic cut-off interval weighted for the corresponding fractional live time (Adriani et al. [19]).

5. Systematic uncertainties

The contributions to the systematic uncertainties in the deuteron measurements are the following:

- Uncertainty on the selection efficiency: this is the statistical error due to the finite size of the efficiency sample. This error was considered and propagated as a systematic uncertainty. For time-dependent efficiencies, time-dependent systematic uncertainties were introduced. The total uncertainty goes from 1% in 2006 to around 3% in 2014 due to the decrease in the statistics.
- Subtraction of contamination of fragmentation products: the disagreement between flight and simulated triton counts was considered an upper systematic uncertainty affecting the secondary particle production from ^{4}He fragmentation in the simulation. This uncertainty is about 2% at 0.6 GV and decreases to about 1% above 1.5 GV.
- Intrinsic accuracy of the unfolding procedure: this was estimated in simulation by reconstructing a known input spectral shape with the unfolding procedure from the corresponding spectrum measured in the tracking system. This procedure was repeated several times by varying the input spectral shape, and the resulting unfolded spectra differed from the input spectra mostly below 1 GV with a maximum difference of about 1.3%, at 0.65 GV.
- The integral of the double-Gaussian distribution, fitting the $1/\beta$ distribution, systematically underestimated the total number of events. This discrepancy was constant, at a level of about 2%, and was used as a systematic uncertainty of the estimated deuteron counts above 2 GV.

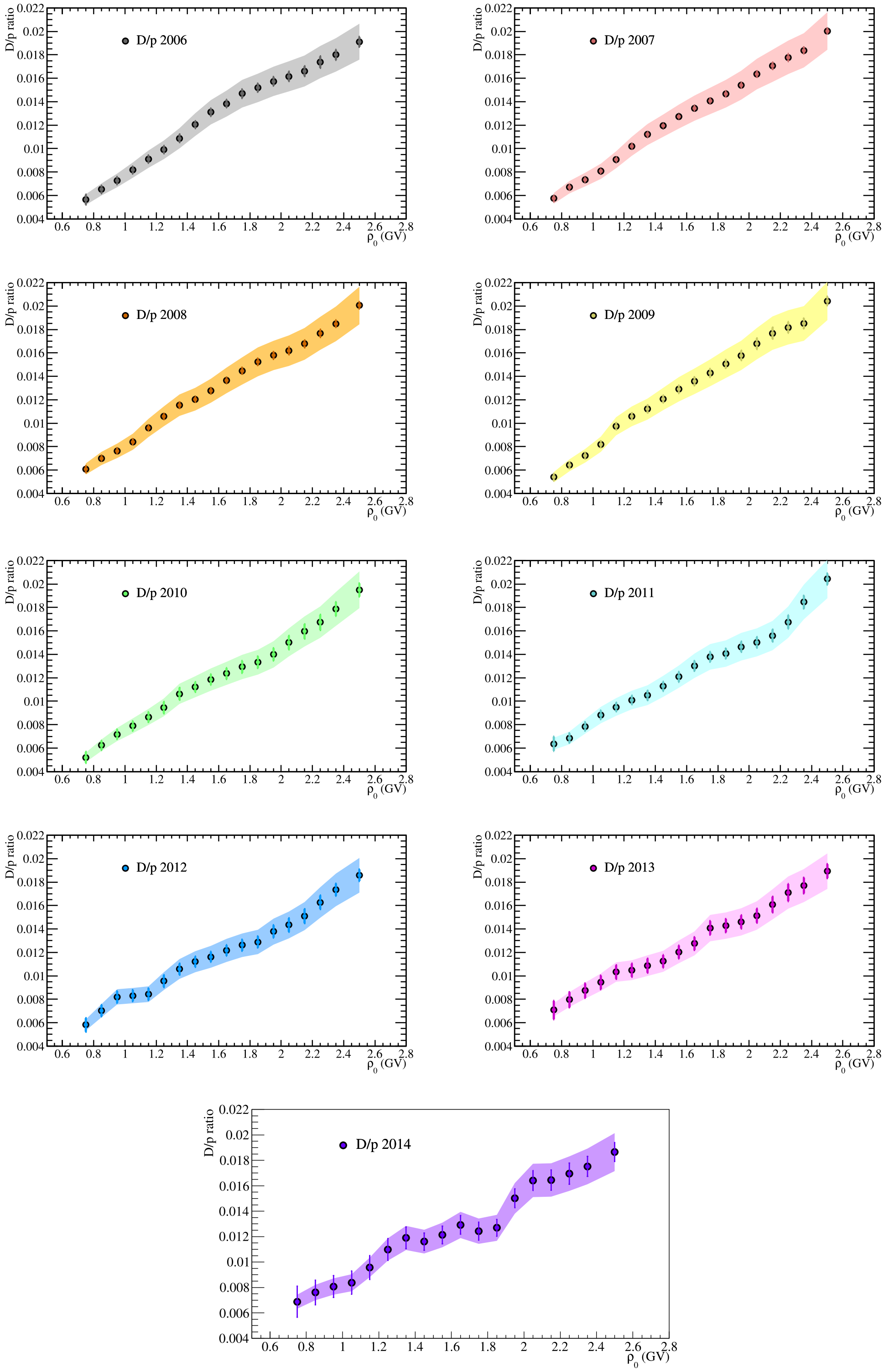

Fig. 10. Yearly averaged D/p flux ratios as a function of the rigidity. Not visible statistical errors bars are smaller than the symbols. The shaded area represents the systematic uncertainties.

- The uncertainty in the effective geometric factor estimated from the Monte Carlo simulation is 0.18% [17], practically independent of energy.

The analysis procedure was validated with the PAMELA Monte Carlo. An input deuteron energy spectrum was simulated at the top of the payload, and the events were propagated into the detectors. The simulated events that satisfied the experimental trigger conditions were saved. Then, deuteron candidates were selected as in Section 3. Selection efficiencies were estimated as in Section 4.1, and a deuteron energy spectrum was evaluated similarly to Section 4.7, except for live

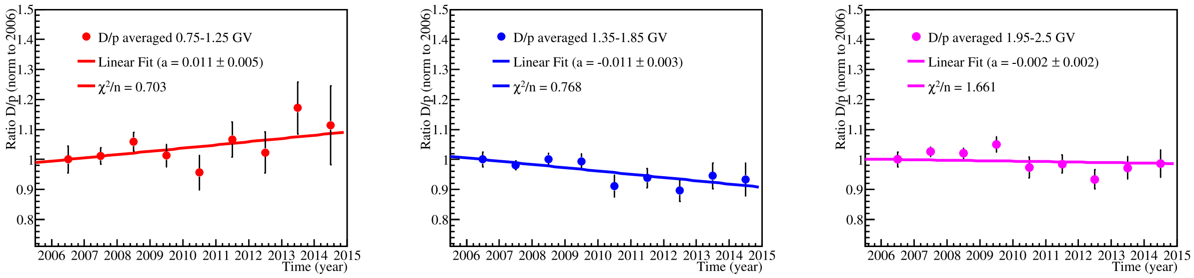

Fig. 11. The yearly D/p flux ratios normalized to the 2006 D/p flux ratio. The solid line represent a linear fit. Left: flux ratios averaged between 0.75 and 1.25 GV, middle: flux ratios averaged between 1.35 and 1.85 GV, right: flux ratios averaged between 1.95 and 2.5 GV. .

time. This resulting spectrum was compared with the input one. Considering statistical uncertainties and previously described systematic uncertainties, the spectra were consistent. Therefore, there was no need for additional systematic uncertainty.

6. Results

Nine yearly rigidity spectra for CR deuterons were obtained for the period between July 2006 and September 2014. These spectra are shown in Fig. 8 as a function of rigidity. Fig. 9 shows the flux D as a function of time for three different rigidities. The solar modulation effect is observed in the time dependence of the fluxes: they gradually increased from 2006 to 2009, approaching the solar minimum of the 23rd solar cycle, and then they progressively decreased, reaching a minimum value in 2014, soon after the solar maximum. The flux at the lowest rigidity showed the highest variations, where the flux increased by ~ 1.85 from 2006 to 2009 and then decreased by ~ 5 in 2014. At higher rigidity values, the variations were less significant; at 2.05 GV, the increase and decrease factors were 1.4 and 2, respectively. The comparison with the yearly averaged spectra obtained from the published AMS-02 D spectrum [13] is also shown. The 2011 AMS-02 D spectrum were obtained averaging the period from 20 May 2011 to 16 December 2011, the 2012 by averaging the period from 17 December 2011 to 4 November 2012, the 2013 by averaging the period from 5 November 2012 to 10 January 2014 and the 2014 refers to the period from the 7 February 2014 to the 25 May 2014.

The shape of the deuteron spectrum was also observed to change over time as an effect of the solar modulation, as evident in Fig. 8. The spectrum became progressively softer from 2006 to 2009 as more low-energy particles could reach the Earth during the solar minimum phase. Consequently, the spectral peak (i.e., the turning point in the value of the maximum flux of each spectrum) shifted from higher to lower rigidities: in 2006, the deuteron spectral peak was located at 1.65 GV, gradually decreasing to 1.45 GV in 2009. In the following years, this trend was reversed because fewer low-energy deuterons could reach the Earth due to the increasing solar activity. Consequently, the observed spectra became progressively harder; however, a precise estimation of the spectral peak is difficult due to the significant systematic effects present in the fluxes at higher rigidities (> 1.8 GV) after 2009.

The deuteron-to-proton (D/p) flux ratios were also evaluated as a function of rigidity and time and are shown in Fig. 10. The p fluxes were obtained by averaging the published PAMELA hydrogen fluxes [17,18] and subtracting the D fluxes reported in this work. It can be noted that the ratios increase by about a factor of 3 as the rigidity increases, probably reflecting the difference in the LIS shapes of protons and deuterons.

The time dependence of the deuteron-to-proton flux ratios averaged between 0.75 and 1.25 GV (left panel), between 1.35 and 1.85 GV (middle panel) and between 1.95 and 2.5 GV (right panel) is shown in Fig. 11, where the ratios were normalized to the values measured in 2006. The solid line represents a fit to the data performed with a polynomial of the first degree:

$$D/p = 1 + a(x - 2006) \tag{4}$$

The value of the fitted parameter a is shown in the legend. Between 0.75 and 1.25 GV, the ratios were observed to assume higher values during the solar maximum phase, up to a factor of 15% higher in 2013 and 2014. The a parameter from the fit shows a value that is different from zero at a level of 2.2 sigma. Between 1.35 and 1.85 GV, the ratios decrease during the solar maximum phase of about 8% with an a parameter from the fit showing a value different from zero at a level of 3.6 sigma. At the highest rigidity, the ratio shows no time dependence and a is compatible with zero.

7. Conclusions

New results on the time evolution of the deuteron spectrum measured with the PAMELA experiment were presented. The deuteron fluxes were obtained with data collected between July 2006 and September 2014 in the rigidity range $[0.7;\ 2.6]$ GV. The fluxes show the expected anticorrelation with the solar activity, increasing during the solar minimum phase and decreasing as the solar activity approached its maximum.

The deuteron-to-proton flux ratio shows a rigidity dependence, increasing as the rigidity increases. The ratio also shows a time dependence between 0.75 and 1.25 GV, with a sigma level of 2.2, increasing from 2006 to 2014 and decreasing between 1.35 and 1.85 GV with a sigma level of 3.3. At the highest rigidities, between 1.35 and 2.5 GV, the ratio shows no time dependence. A time-dependent ratio could result from the different mass-to-charge ratios and shapes of the respective LIS.

In conclusion, these results are particularly relevant for solar-modulation studies covering most of a solar cycle from minimum to maximum activity, including a change in solar magnetic polarity in 2013. The observations presented in this work offer an opportunity to study the effects of deuteron isotopic mixing in the observed proton-to-helium ratios in detail. The results presented in this work will be available at the Cosmic Ray Data Base of the ASI Space Science Data Center (http://tools.asdc.asi.it/CosmicRays/chargedCosmicRays.jsp).

We acknowledge partial financial support from Agenzia Spaziale Italiana, Italy (ASI). We also acknowledge support from Deutsches Zentrum fur Luft- und Raumfahrt (DLR), The Swedish National Space Board, The Swedish Research Council. We acknowledge financial support from the Italian foreign minister in the context of “Programma Esecutivo Italia – Sud Africa” (code ZA23MO02). R.M. acknowledges partial financial support from the INFN Grant “giovani”, project AS-MDM.

CRediT authorship contribution statement

R. Munini: Supervision, Formal analysis, Conceptualization.

Declaration of competing interest

The authors declare the following financial interests/personal relationships which may be considered as potential competing interests: Riccardo Munini reports financial support was provided by Government of Italy Ministry of Foreign Affairs and International Cooperation. If there are other authors, they declare that they have no known competing financial interests or personal relationships that could have appeared to influence the work reported in this paper.

Data availability

Data will be made available on request.

References

[1] W. Webber, Adv. Space Res. 19 (1997) 755–758, http://dx.doi.org/10.1016/S0273-1177(96)00141-X.

[2] B. Coste, L. Derome, D. Maurin, A. Putze, AeA 539 (2012) A88, http://dx.doi.org/10.1051/0004-6361/201117927.

[3] N. Tomassetti, Astrophys. Space Sci. 342 (2012) 131–136, http://dx.doi.org/10.1007/s10509-012-1138-y.

[4] J. Wu, H. Chen, Phys. Lett. B 789 (2019) 292–299, http://dx.doi.org/10.1016/j.physletb.2018.11.052.

[5] D.M. Gomez-Coral, C. Gerrity, R. Munini, P. von Doetinchem, Phys. Rev. D 107 (2023) 123008, http://dx.doi.org/10.1103/PhysRevD.107.123008.

[6] W. Webber, et al., Astrophys. J. 380 (1991) 230–234, http://dx.doi.org/10.1086/170578.

[7] G. de Nolfo, et al., AIP Conf. Proc. 528 (2000) 425–428, http://dx.doi.org/10.1063/1.1324352.

[8] E.A. Bogomolov, G.I. Vasilev, S.Y. Krutkov, S.V. Stepanov, M.S. Shulakova, Bull. Russ. Acad. Sci. Phys. 67 (2003) 487–492.

[9] J. Wang, et al., Astrophys. J. 564 (2002) 244–259, http://dx.doi.org/10.1086/324140.

[10] P. Papini, et al., Astrophys. J. 615 (2004) 259–274, http://dx.doi.org/10.1086/424027.

[11] M. Aguilar, et al., Phys. Rep. 366 (2002) 331–405, http://dx.doi.org/10.1016/S0370-1573(02)00013-3.

[12] O. Adriani, et al., Astrophys. J. 818 (1) (2016a) 68, http://dx.doi.org/10.3847/0004-637X/818/1/68.

[13] M. Aguilar, B. Alpat, G. Ambrosi, et al., Phys. Rev. Lett. 132 (2024) 261001, http://dx.doi.org/10.1103/PhysRevLett.132.261001.

[14] M. Potgieter, Living Rev. Sol. Phys. 10 (2013) http://dx.doi.org/10.12942/lrsp-2013-3.

[15] G. Bazilevskaya, et al., Space Sci. Rev. 186 (2014) 409–435, http://dx.doi.org/10.1086/170578.

[16] P. Picozza, A.M. Galper, G. Castellini, et al., Astropart. Phys. 27 (2007) 296–315, http://dx.doi.org/10.1016/j.astropartphys.2006.12.002.

[17] O. Adriani, G.C. Barbarino, G.A. Bazilevskaya, et al., ApJ 765 (2013) 91, http://dx.doi.org/10.1088/0004-637X/765/2/91.

[18] M. Martucci, R. Munini, M. Boezio, et al., ApJL 854 (2018) L2, http://dx.doi.org/10.3847/2041-8213/aaa9b2.

[19] O. Adriani, et al., ApJ 810 (2015) 142, http://dx.doi.org/10.1088/0004-637X/810/2/142.

[20] O. Adriani, G.C. Barbarino, G.A. Bazilevskaya, et al., Phys. Rev. Lett. 116 (24) (2016b) 241105, http://dx.doi.org/10.1103/PhysRevLett.116.241105.

[21] N. Marcelli, M. Boezio, A. Lenni, et al., Astrophys. J. 893 (2) (2020) 145, http://dx.doi.org/10.3847/1538-4357/ab80c2.

[22] N. Marcelli, M. Boezio, A. Lenni, et al., Astrophys. J. Lett. 925 (2) (2022) L24, http://dx.doi.org/10.3847/2041-8213/ac4787.

[23] O. Adriani, et al., Astrophys. J. 770 (2013) 2, http://dx.doi.org/10.1088/0004-637X/770/1/2.

[24] O. Adriani, et al., Phys. Rep. 544 (2014) 323–370, http://dx.doi.org/10.1016/j.physrep.2014.06.003.

[25] O. Adriani, et al., Riv. Nuovo Cimento 40 (10) (2017) 473–522, http://dx.doi.org/10.1393/ncr/i2017-10140-x.

[26] T. Erwan, C. Finlay, C. Beggan, et al., Earth, Planets Space 67 (2015) 79, http://dx.doi.org/10.1186/s40623-015-0228-9.

[27] S. Agostinelli, J. Allison, K. Amako, et al., Nucl. Instrum. Methods Phys. Res. Sect. A: Accel. Spectrometers, Detect. Assoc. Equip. 506 (3) (2003) 250–303, http://dx.doi.org/10.1016/S0168-9002(03)01368-8.

[28] G. D'Agostini, Nucl. Instrum. Methods Phys. Res. A 362 (1995) 487–498, http://dx.doi.org/10.1016/0168-9002(95)00274-X.

[29] O. Adriani, G.C. Barbarino, G.A. Bazilevskaya, et al., Science 332 (2011) 69, http://dx.doi.org/10.1126/science.1199172.